EARTHQUAKE ENGINEERING AND STRUCTURAL DYNAMICS, VOL. 16, 523–539 (1988)

TRANSIENT PRESSURES IN HYDROTECHNICAL TUNNELS DURING EARTHQUAKES

SLOBODAN B. KOJIĆ*

University of Southern California, Los Angeles, CA, U.S.A., and Energoproject Co., Belgrade, Yugoslavia

AND

MIHAILO D. TRIFUNAC†

Department of Civil Engineering, University of Southern California, Los Angeles, CA, U.S.A.

SUMMARY

Transient pressures generated by earthquake shaking in hydrotechnical tunnels are evaluated by the discrete Fourier transform technique. The effects of the horizontal ground motion accelerating the closed downstream tunnel gate, as well as the upstream dam face, and the influence of the vertical motion of the reservoir floor are considered in this analysis. An example of a typical bottom outlet is analysed by subjecting it to several computed accelerograms. It is shown that high hydrodynamic pressures can be developed, several times larger than the hydrostatic pressure.

INTRODUCTION

Hydrotechnical tunnels, penstock and bottom outlets are common elements in many dam projects. Their functions are to provide efficient and economical means of releasing the water from the reservoir according to the desired downstream use for irrigation or for power generation. The conduits which lead the water to the turbines are usually designed to withstand high hydraulic transient pressures arising in various turbine operations. Surge tanks are frequently used to protect the upstream part of the conduit. For such systems there is little need for analysis of hydrodynamic pressures due to earthquakes, although some pressure increase may be expected. However, hydrotechnical tunnels and bottom outlets for irrigation purposes usually are not designed for waterhammer effects like the turbine penstocks. In most cases such tunnels do not have surge tanks or other openings, which would damp the transient pressures caused by an earthquake. Usually, they may have valves or gates located at the upstream intake, at an intermediate point and at the downstream end. Owing to various downstream demands, it may happen that the intermediate or the end gates are closed for long periods of time, leaving the upstream conduit part under a full reservoir pressure. Under such conditions in seismically active regions, an earthquake may cause the water pressure to increase or decrease with respect to the hydrostatic pressure or steady pressure conditions. Understanding of the transient hydrodynamic pressure caused by earthquakes is of interest for the proper design approach to these structures. Failure of the hydrotechnical tunnel during an earthquake can initiate erosion of surrounding material and consequently, depending where a break occurs, it may cause increased uplift under the dam, dam abutment failure, stilling basin or spillway damage, hydroelectric power plant break or a crash of any other vital component of the dam system. Any of these events can be a starting point for a dam collapse.

Zienkiewicz[1] was among the first to point out the resonant effects in the bottom outlets due to harmonic horizontal motion of the downstream gate. On a specific project Obradović[2] carried out an earthquake

* Research Fellow, University of Southern California, and Staff Member, Energoproject Co.
† Professor of Civil Engineering.

0098–8847/88/040523–17$08.50

Received 13 May 1987
Revised 6 October 1987

response analysis of water in the bottom outlet. His model has included only horizontal downstream gate motion in the generation of hydrodynamic pressures due to earthquakes. The method used in his analysis is the method of characteristics. The results showed that high hydrodynamic pressures can be developed during an earthquake and that these depend on earthquake amplitude and frequency content.

The present analysis has the following objectives.

(a) To illustrate the additional effects of upstream boundary conditions, i.e. the influence of hydrodynamic pressures developed during earthquake response of dam and reservoir floor on generation of transient pressures along the bottom outlet. For simplicity, the dam will be considered as rigid, although, in some cases, its flexibility may not be ignored. Inclusion of the dam flexibility is possible via finite element discretization of the dam, for example, but it will not be studied here. The reservoir and the water in the conduit are assumed to be compressible. The downstream boundary condition, horizontally moving gate, has been included also.

(b) To demonstrate the possibility of using the method of discrete Fourier transform in a hydraulic transient problem via the fast Fourier transform algorithm.

(c) To examine the capabilities of the mathematical model and of the proposed numerical technique on a realistic bottom outlet model.

DESCRIPTION OF THE BOTTOM OUTLET

The bottom outlets carry water from the reservoir to the river or to the irrigation channels downstream. A simplified schematic of this structure, with the dam and the stilling basin, is shown in Figure 1. The bottom

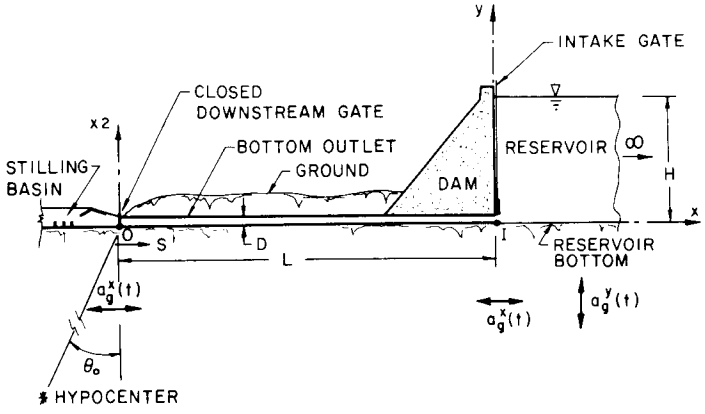

(a) SECTION A - A

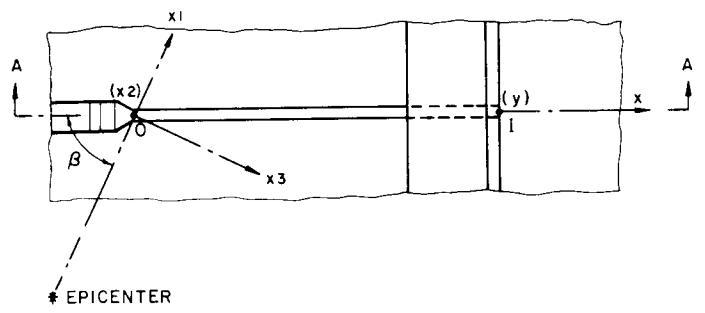

(b) LAYOUT

Figure 1. Bottom outlet, dam and reservoir with earthquake ground accelerations: a_g^x and a_g^y

outlet intake is usually located at the bottom of the reservoir close to the dam upstream face. The intake sliding gate stops water flow when the bottom outlet is serviced or repaired. An intermediate valve helps in closing of the intake gate. The downstream gate regulates the water discharge according to the downstream requirements. Before entering into the river the water is passed through the stilling basin whose role is to decrease the water velocity. The cross section of the conduit is usually circular and it is made of reinforced concrete. The conduit may be lined by steel, if water velocities and pressures are high.

The gates, concrete and steel lining are, in general, dimensioned to withstand the full reservoir pressure. Only the intermediate valve is checked for hydrodynamic effects to enable its closure in the flowing water with high velocity.

If the dam is located in a seismically active region, it is of interest for the general dam safety to determine the hydrodynamic, transient pressure along the bottom outlet during an earthquake. The case when the downstream gate is closed and the bottom outlet is under the full reservoir pressure will be considered. Without loss of generality the bottom outlet axis is assumed to be perpendicular to the dam upstream face. Under these conditions the whole system, the dam, the reservoir bottom and the downstream gate, is exposed to the ground motion.

THE MATHEMATICAL MODEL AND THE SOLUTION PROCEDURE

One-dimensional wave equation for viscous flow

The hydrodynamic pressure associated with small amplitude, irrotational, one-dimensional motion, and for water assumed to be linearly compressible and viscous, is described by the following wave equation:[3]

$$\frac{\partial^2 p}{\partial s^2} = \frac{1}{c^2}\frac{\partial^2 p}{\partial t^2} + R\frac{\partial p}{\partial t} \tag{1}$$

where $p(s, t)$ is the hydrodynamic pressure, in excess of hydrostatic pressure, along the bottom outlet, as a function of the space coordinate s and time t, c is compression wave velocity in water, and R describes friction losses.

Equation (1) is called the waterhammer equation and it is used in hydraulic engineering for analysis of unsteady, transient flow through closed conduits.[3] The friction R is assumed to be the same as for the steady-state flow in conduits, i.e. the Darcy–Weisbach formula is used for computing the friction losses. R will be presented in this transient problem, caused by an earthquake, in a somewhat different form to that which is normally used in waterhammer analysis (mean discharge[3] is assumed to be equal to zero). For laminar flow, R can be shown to be

$$R = \frac{32v}{c^2 D^2} \tag{2}$$

and for turbulent flow,

$$R = \frac{fv}{c^2 D} \tag{3}$$

where $v = \mu/\rho$, the kinematic viscosity, μ is the absolute water viscosity, ρ is the water mass density, D is the conduit diameter, f is the friction factor dependent on the conduit roughness and Reynolds number (it can be determined from the Moody diagram[4]), and v is the water particle velocity in the conduit. Thus, the hyperbolic partial differential equation (1) is linear for laminar flow and non-linear for turbulent flow.

The water particle velocity v is assumed to be equal to the ground velocity induced by an earthquake. The earthquake ground motion accelerates the downstream gate, the dam and reservoir bottom and they all generate the pressure waves which propagate through the bottom outlet.

A representative Reynolds number, for the peaks of the smallest recorded earthquake velocities (Trifunac and Brady,[5] $v \approx 0{\cdot}01$ m/s), and for the small bottom outlet diameters ($D = 0{\cdot}5$ m), is about 4000. This suggests

that the water motion can be turbulent. However, during earthquake shaking the water velocity is expected to change sign frequently, while it oscillates about zero. Consequently, it may be assumed that most of the time the water motion will be laminar. Therefore, R defined by equation (2), and the description of the pressure change given by the linear version of equation (1), will be used.

The non-linear waterhammer equation, presented by Streeter and Wylie[4] in a somewhat different form, can be solved by the method of characteristics. A solution is given in the time domain with an approximate integration of the friction term.

Some experiments and analyses[2] have shown that the influence of water friction in the hydraulic transient problems is not very significant for the amplitudes of the hydrodynamic pressures. However, the small viscous term in equation (1) is retained to improve numerical stability and the efficiency of the method applied for the solution.

Method of solution: The Fourier transform technique

Equation (1) for the laminar flow can be solved by the method of Fourier transforms. This method uses a property of linear time-invariant systems that, for the steady-state harmonic excitation, the response is also the steady-state harmonic motion at the same frequency.[6] So, if the harmonic excitation is the real part of $e^{i\omega t}$, then the response $p^l(s, t)$ is the real part of $\bar{p}^l(s, \omega)e^{i\omega t}$, where $\bar{p}^l(s, \omega)$ is the complex frequency response function which describes the frequency dependence of the response amplitude and phase. Once this function $\bar{p}^l(s, \omega)$ has been obtained for a range of frequencies, the response to an arbitrary ground motion $a_g^l(t)$ can be obtained by the Fourier synthesis of the responses to the individual harmonic components, i.e.

$$p^l(s, t) = \frac{1}{2\pi} \int_{-\infty}^{\infty} \bar{p}^l(s, \omega) A_g^l(\omega) e^{i\omega t} d\omega \tag{4}$$

where
i is the imaginary unit, $l = x, y$ are the horizontal and vertical components of ground motion, and $A_g(\omega)$ is the Fourier transform of $a_g^l(t)$,

$$A_g^l(\omega) = \int_0^{T_d} a_g^l(t) e^{-i\omega t} dt \tag{5}$$

T_d is the duration of the ground motion. The total response $p(s, t)$ to simultaneous horizontal and vertical components of ground motion is obtained as

$$p(s, t) = p^x(s, t) + p^y(s, t) \tag{6}$$

Evaluation of the integrals given by equations (4) and (5) is performed in discrete form, using the fast Fourier transform (FFT) algorithm.[7]

Boundary conditions

The downstream gate is assumed to be vertical, flat and rigid. Ground motion is assumed to be transferred directly to this gate. Under these conditions the hydrodynamic pressure for $s = 0$, at the gate, can be expressed as

$$\frac{\partial p(0, t)}{\partial s} = -\rho a_g^l(t), \quad l = x \tag{7}$$

This equation follows from D'Alembert's principle applied to an infinitesimal fluid element at the interface between water and the gate.

At the intake $s = L$, the hydrodynamic pressures in the bottom outlet and the reservoir are the same:

$$p(L, t) = p_R^x(\bar{x}, \bar{y}, t) + p_R^y(\bar{x}, \bar{y}, t) \tag{8}$$

where $p_R^{x,y}(\bar{x}, \bar{y}, t)$ is the hydrodynamic pressure in the reservoir at the intake of bottom outlet, with coordinates $(\bar{x}, \bar{y})$, due to horizontal or vertical ground motion.

Chopra and his co-workers[8,9] analysed generation of the hydrodynamic pressures in the reservoir due to the dam and reservoir bottom motion during earthquakes. In this illustration of the bottom outlet pressures, the dam will be assumed to be rigid and with vertical upstream face and the solution given by Fenves and Chopra,[9] and by Rosenblueth[10] will be used for approximate determination of $p_R^I(, x, y, t)$. A more refined determination of $p_R^I(x, y, t)$ would require the three-dimensional analysis of the dam and waves propagating through the basement and reservoir.

The hydrodynamic pressure in the reservoir, $p_R^I(x, y, t)$, in excess of the hydrostatic pressure, is governed by the two-dimensional wave equation which is valid for small, irrotational, inviscid motion,

$$\frac{\partial^2 p_R}{\partial x^2} + \frac{\partial^2 p_R}{\partial y^2} = \frac{1}{c^2}\frac{\partial^2 p_R}{\partial t^2} \tag{9}$$

where c is the velocity of sound in water. The pressure gradient at the vertical, upstream dam face is

$$\frac{\partial p_R}{\partial x}(0, y, t) = -\rho a_g^x(t) \tag{10}$$

By approximate modelling of the interaction between the reservoir water and the reservoir bottom, considering only the vertically propagating pressure waves, the boundary condition at that interface can then be expressed as follows:

$$\frac{\partial p_R}{\partial y}(x, 0, t) - q\frac{\partial p_R}{\partial t}(x, 0, t) = \rho a_g^y(t) \tag{11}$$

where $q = \rho/(\rho_F c_F)$ and $c_F = \sqrt{(E_F/\rho_F)}$. E_F is the Young's modulus of elasticity and ρ_F is the mass density of the reservoir bottom material.

At the free surface the following condition is satisfied:

$$p_R(x, H, t) = p_{atm} \tag{12}$$

and without loss of generality $p_{atm} = 0$.

The governing equation (9) and the boundary conditions, equations (10), (11) and (12), are linear and the same solution technique, explained previously, can be applied. The hydrodynamic pressure $p_R^x(x, y, t)$ within the reservoir domain due to harmonic horizontal ground motion $a_g^x = 1\,e^{i\omega t}$, is

$$p_R^x(x, y, t) = 2\rho H \sum_{n=1}^{\infty} \frac{\lambda_n^2 I_n \psi_n(y)\, e^{-\kappa_n x}}{[H(\lambda_n^2 - \omega^2 g^2) + i\omega g]\,\kappa_n} e^{i\omega t} \tag{13}$$

where λ_n and ψ_n are complex valued and frequency dependent eigenvalues and eigenfunctions respectively of the impounded reservoir water. They are given by the following equations:

$$e^{2i\lambda_n H} = -\frac{\lambda_n - \omega q}{\lambda_n + \omega q}, \quad n = 1, 2, 3, \ldots . \tag{14}$$

and

$$\psi_n(y) = \frac{(\lambda_n - \omega q)\, e^{-i\lambda_n y} + (\lambda_n + \omega q)\, e^{i\lambda_n y}}{2\lambda_n}, \quad n = 1, 2, 3, \ldots \tag{15}$$

I_n is defined as an integral of the eigenfunction, over the reservoir depth, i.e.

$$I_n = \frac{1}{H}\int_0^H \psi_n(y)\,dy, \qquad n = 1, 2, 3, \ldots \tag{16}$$

and κ_n is given by

$$\kappa_n = \lambda_n^2 - \omega^2/c^2, \qquad n = 1, 2, 3, \ldots \tag{17}$$

The exponential function $e^{-\kappa_n x}$ decreases pressure with increasing x, because of the assumption of an infinite reservoir in the upstream direction.

For the vertical harmonic motion of the reservoir bottom, $a_g^y(t) = 1\,e^{i\omega t}$, the hydrodynamic pressure in the reservoir is

$$p_R^y(x, y, t) = \rho c \frac{\sin\frac{\omega}{c}(H-y)}{\omega\cos\left(\frac{\omega}{c}H\right) + icq\sin\left(\frac{\omega}{c}H\right)} e^{i\omega t} \tag{18}$$

Equations (13) and (18) without time functions $e^{i\omega t}$ represent the complex frequency response functions $\bar{p}_R(x, y, \omega)$ for hydrodynamic pressure in the reservoir domain. Moduli of these functions are given in Figure 2 for the range up to 25 Hz and for several values of the wave reflection coefficient[9] α defined by

$$\alpha = \frac{1-qc}{1+qc} \tag{19}$$

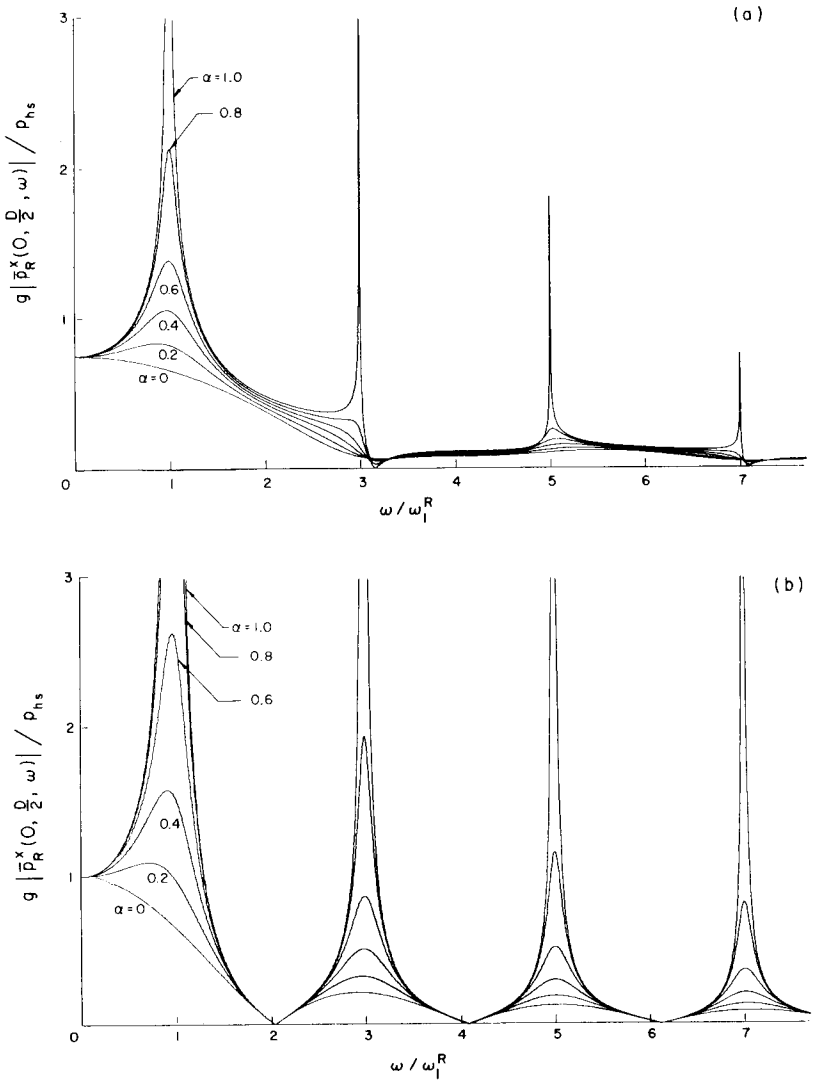

Figure 2. Influence of reservoir bottom absorption on the hydrodynamic pressure in frequency domain at the bottom outlet intake: (a) horizontal motion of the rigid dam; (b) vertical motion of the reservoir floor

This coefficient represents the ratio of the amplitude of the reflected hydrodynamic pressure wave to the amplitude of the vertically propagating pressure wave incident on the reservoir floor. The plotted values are scaled by the hydrostatic pressure and the horizontal frequency axis is scaled by the fundamental reservoir frequency.

Complex valued frequency response function for bottom outlet

The hydrodynamic pressure along the bottom outlet due to harmonic ground motion can be expressed as

$$p^l(x, t) = \bar{p}^l(s, \omega)\mathrm{e}^{\mathrm{i}\omega t}, \quad l = x, y \tag{20}$$

The complex valued frequency response function $\bar{p}^l(s, \omega)$ is obtained by solving equation (1), with the boundary conditions expressed by equations (7) and (8).

Substituting equation (20) into equation (1) yields the one-dimensional Helmholtz equation

$$\bar{p}^{l''}(s, \omega) + \left(\frac{\omega^2}{c^2} - \mathrm{i}\omega R\right)\bar{p}^l(s, \omega) = 0 \tag{21}$$

The solution of equation (21) is

$$\bar{p}^l(s, \omega) = C_1^l(\omega)\mathrm{e}^{ws} + C_2^l(\omega)\mathrm{e}^{-ws}, \quad l = x, y \tag{22}$$

where w is given by

$$w = \sqrt{\left(-\frac{\omega^2}{c^2} + \mathrm{i}\omega R\right)} \tag{23}$$

The coefficients $C_1^l(\omega)$ and $C_2^l(\omega)$ are determined from the boundary conditions. Satisfying the boundary condition at the downstream gate, expressed by equation (7), for harmonic ground motion $a_g^x(t) = 1\,\mathrm{e}^{\mathrm{i}\omega t}$, leads to

$$C_2^l(\omega) = \frac{\rho}{w} + C_1^l(\omega), \quad l = x, y \tag{24}$$

Applying the upstream boundary condition given by equation (8) yields

$$C_1^l(\omega) = \frac{w\,\mathrm{e}^{wL}\bar{p}_R^l(\bar{x}, \bar{y}, \omega) - \rho}{w(1 + \mathrm{e}^{2wL})} \tag{25}$$

where $\bar{p}_R^l(\bar{x}, \bar{y}, \omega)$ is evaluated by equation (13) or (18). Thus, for horizontal ground motion, the complex valued frequency response function for the hydrodynamic pressure along the bottom outlet is given by

$$\bar{p}^x(s, \omega) = \left\{[w\,\mathrm{e}^{wL}\bar{p}_R^x(\bar{x}, \bar{y}, \omega) - \rho]\frac{1 + \mathrm{e}^{2ws}}{w(1 + \mathrm{e}^{2wL})} + \frac{\rho}{w}\right\}\mathrm{e}^{-ws} \tag{26}$$

and due to vertical ground motion, equation (22) combined with equations (24) and (25), for $l = y$, yields

$$\bar{p}^y(s, \omega) = \frac{\mathrm{e}^{wL}(1 + \mathrm{e}^{2ws})}{\mathrm{e}^{-ws}(1 + \mathrm{e}^{2wL})}\bar{p}_R^y(\bar{x}, \bar{y}, \omega) \tag{27}$$

EXAMPLE

To illustrate this computational procedure, the bottom outlet, shown in Figure 1 (similar to the one constructed on the Chira-Piura Project in Peru), has been chosen as an example. The bottom outlet has a diameter $D = 4{\cdot}0$ m and length $L = 300$ m. At the intake the depth of reservoir is $H = 100$ m. The compression wave velocity of the water in the bottom outlet as well as in the reservoir is assumed to be the same, $c = 1300$ m/s.

The complex valued frequency response functions $\bar{p}^l(s, \omega)$ are computed for the range up to 25 Hz, at five

sections, each located at a quarter length of the bottom outlet, and for three different cases of the unit harmonic excitations. In the first case, shown in Figure 3(a), the downstream gate accelerates horizontally while the dam and the reservoir floor do not move. The second case, shown in Figure 3(b), represents the horizontal motion of the rigid dam without moving the downstream gate and the reservoir floor. Vertical motion of the reservoir bottom corresponds to the third case of the unit harmonic excitation, and is shown in Figure 3(c), with no motion of the downstream gate and the dam. The plots in Figure 3 represent the moduli of $\bar{p}^i(s, \omega)$ scaled by the hydrostatic pressure p_{hs}. The frequency axis is scaled by the fundamental frequency of the bottom outlet ω_1^{BO}.

Common features to all frequency response functions are the frequencies where peaks occur. These represent characteristic frequencies of the water in the bottom outlet. For undamped motion they are

$$\omega_n^{BO} = \frac{\pi c}{2L} n, \qquad n = 1, 3, 5, \ldots \tag{28}$$

The characteristic frequencies of the reservoir water with a non-absorbing boundary ($q = 0$) are

$$\omega_n^{R} = \frac{\pi c}{2H} n, \qquad n = 1, 3, 5, \ldots \tag{29}$$

For the chosen parameters, $L = 300$ m and $H = 100$ m, the ratio $\omega_n^R/\omega_n^{BO} = 3$.

The frequency response functions differ in the width at resonant peaks. For the case of the downstream gate moving with unit acceleration, Figure 3(a), the broadest peak is encountered at the fundamental frequency, $\omega_1^{BO} = \pi c/2L$. Unit horizontal rigid dam motion has generated the broadest peak at the second characteristic frequency. This can be expected considering the value of the ratio ω_n^R/ω_n^{BO} and the shape of the reservoir frequency response function, shown in Figure 2(a), for the wave reflection coefficient $\alpha = 0{\cdot}8$ used in this example. Similar effects are observed for the vertical motion of the reservoir floor, Figure 3(c), where broad peaks repeat at each reservoir characteristic frequency [see also Figure 2(b)]. The pressures in the frequency domain also differ in phase.

Ground motions of the two recorded earthquakes, San Fernando of February 9, 1971 at Pacoima Dam, and Kern County of July 21, 1952 at Taft Lincoln School Tunnel, have been used, with some modifications, as excitation functions for the outlet–dam–reservoir system. The modifications are made to represent the effects of the plane P, SV and SH waves propagating through the half space.[11,12] The waves are assumed to come from the earthquake hypocentre in the vertical plane $X1$–$X2$, shown in Figure 1(b), and with incident angle θ_0, which is seen in Figure 1(a). In the horizontal plane $X1$–$X3$ the epicentral azimuth is defined by angle β.

For the purpose of this example, the vertical recorded earthquake component is supposed to be associated only with P, the largest horizontal with SH and another recorded horizontal acceleration with SV waves. All incident components are scaled arbitrarily in such a way that the largest component has the maximum amplitude equal to $0{\cdot}15\,g$. Fourier transforms of those accelerograms, $\bar{a}$, are multiplied by the corresponding transfer functions $\bar{\ddot{U}}_i^{P,SV,SH}$ for accelerations due to P, SV and SH waves given by equations (A17) to (A19) in the Appendix. The simulated accelerograms are then obtained along coordinate axes $X1$, $X2$ and $X3$ by inverse Fourier transform of the resulting functions $\bar{\ddot{U}}_1$. Those are computed at points O and I, shown in Figure 1, for two incident angles: $\theta_0 = 30°$ and $\theta_0 = 60°$. At the point I these accelerograms have accounted for the delay (relative to point O) depending on the incident angle θ_0, the bottom outlet length L and the chosen velocities of longitudinal and transverse waves: $c_L = 2500$ m/s and $c_T = 1450$ m/s, respectively. The resulting horizontal (along the bottom outlet at $\beta = 45°$, Figure 1), and vertical earthquake ground motions at the point O are shown in Figure 4. This set of the simulated accelerograms is used to investigate possible effects of the phase delay of the earthquake motions on the water response in the bottom outlet.

The hydrodynamic pressures in the time domain (for the first 30 s), at five sections along the bottom outlet, are evaluated by using the convolution integral given by equation (4). To preserve the stability of the numerical procedure some investigation of the complex frequency response functions may be necessary. Instability may arise from the sharp peaks at the characteristic frequencies of these functions and from the limited number of discrete points for their description. Stability can be achieved by increasing the number of points required by the FFT algorithm, or by analytic integration in the vicinity of the high peaks of the frequency response

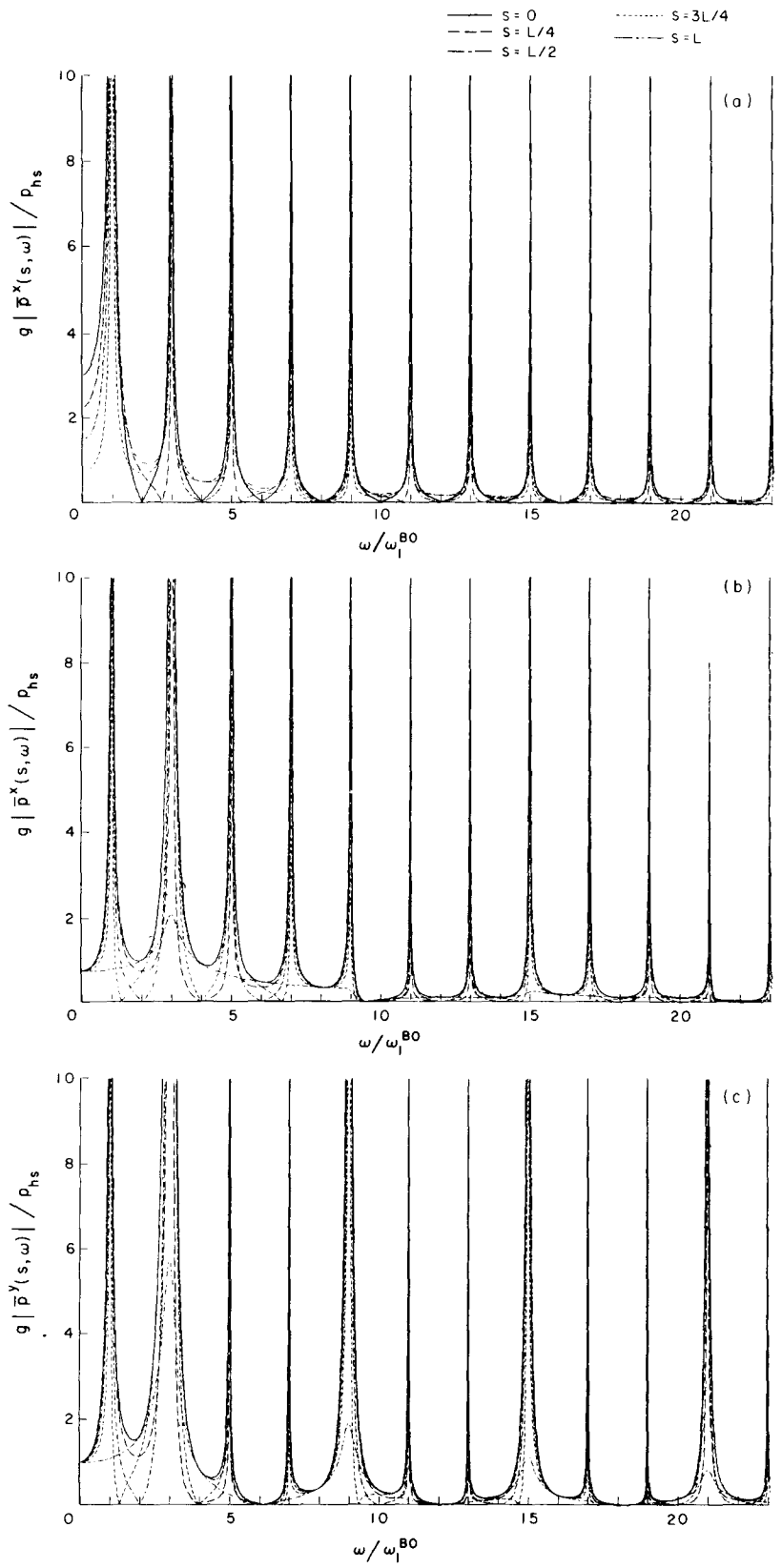

Figure 3. Spatial variations of the hydrodynamic pressure in the frequency domain along the bottom outlet: (a) unit horizontal motion of the downstream gate; (b) unit horizontal motion of the rigid dam; (c) unit vertical motion of the reservoir floor

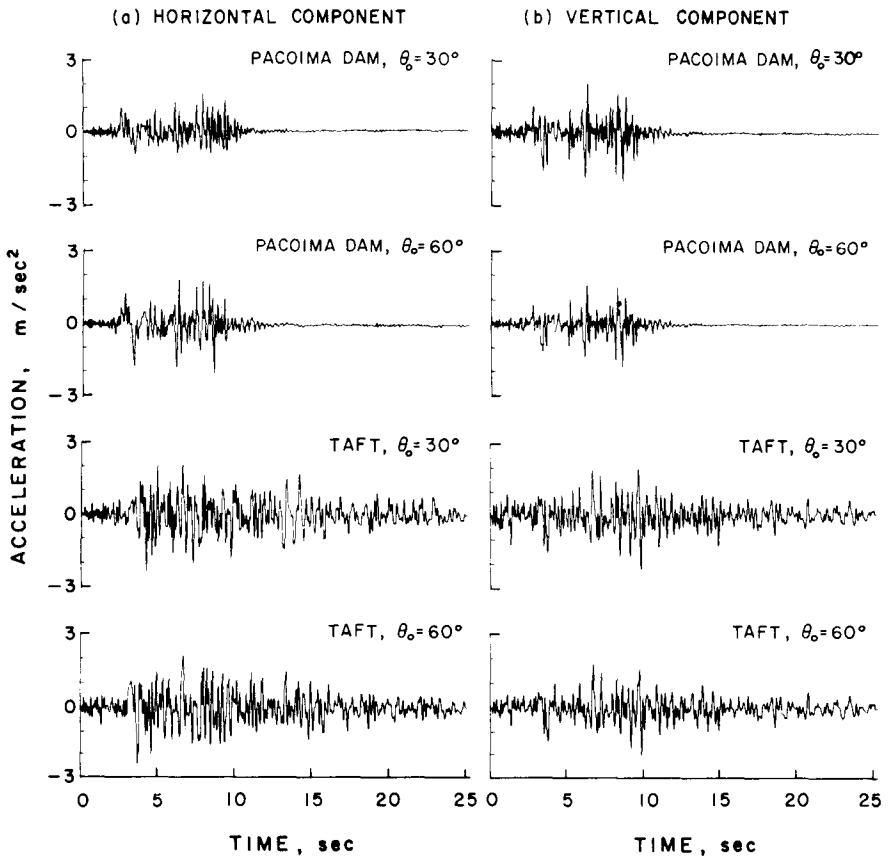

Figure 4. Simulated accelerograms at the downstream gate

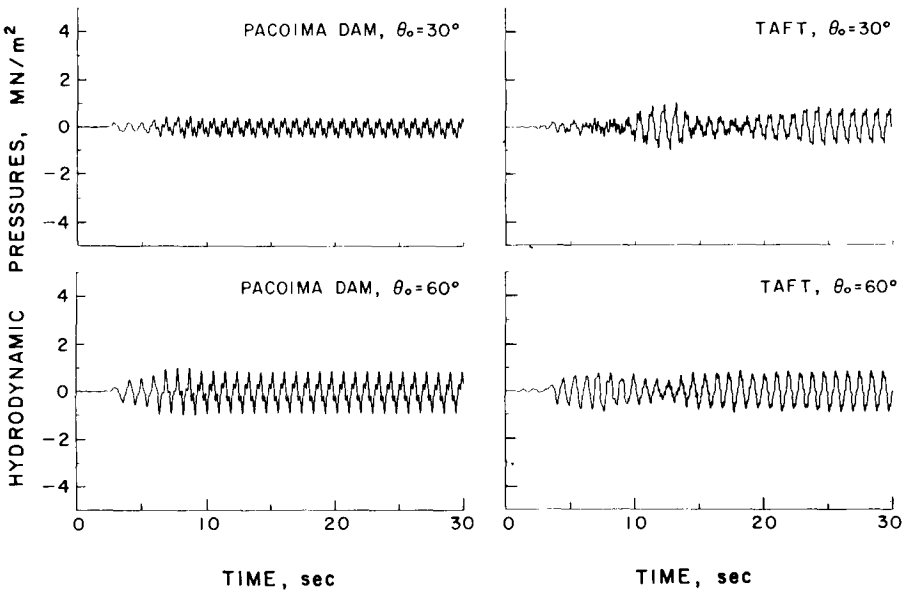

Figure 5. Hydrodynamic pressures at the downstream gate generated by its motion

functions. Stability can be achieved also by increasing R in equation (1), i.e. increasing the water viscosity v slightly above its real value. By doing this, sharp peaks are rounded and only 4096 points are used for description of time or frequency functions and without any significant loss in accuracy of the end results. Even with the increased water viscosity, v, the hydrodynamic pressures, after the end of the excitation, may not decrease much with time. Therefore, the special 'overlap-add'[13] procedure to avoid 'end effects'[13] has been applied.

The computation has been performed separately for each of the three boundary conditions: motion of the downstream gate, the dam motion and the reservoir floor motion. The simulated accelerograms shown in Figure 4(a) are used for the downstream gate excitation. The dam is subjected to two sets of the simulated accelerograms for in-phase [shown in Figure 4(a)] and for phase shifted accelerations (see the Appendix). Similarly, the reservoir bottom is excited by the computed vertical components of accelerograms, for in-phase [shown in Figure 4(b)] and for the phase shifted motions.

Figure 5 shows the variation of the pressure due to the downstream gate motions and associated predominantly with the fundamental frequency of the system, although the presence of the second characteristic frequency is noticeable. For these moderate accelerations (about 0·2 g), the hydrodynamic pressures have reached the value of the hydrostatic pressure (about 1 MN/m^2).

The hydrodynamic pressures caused by the horizontal in-phase acceleration of the dam are shown in Figure 6(a). It is seen that the contributions to the response come mainly from the second characteristic frequency.

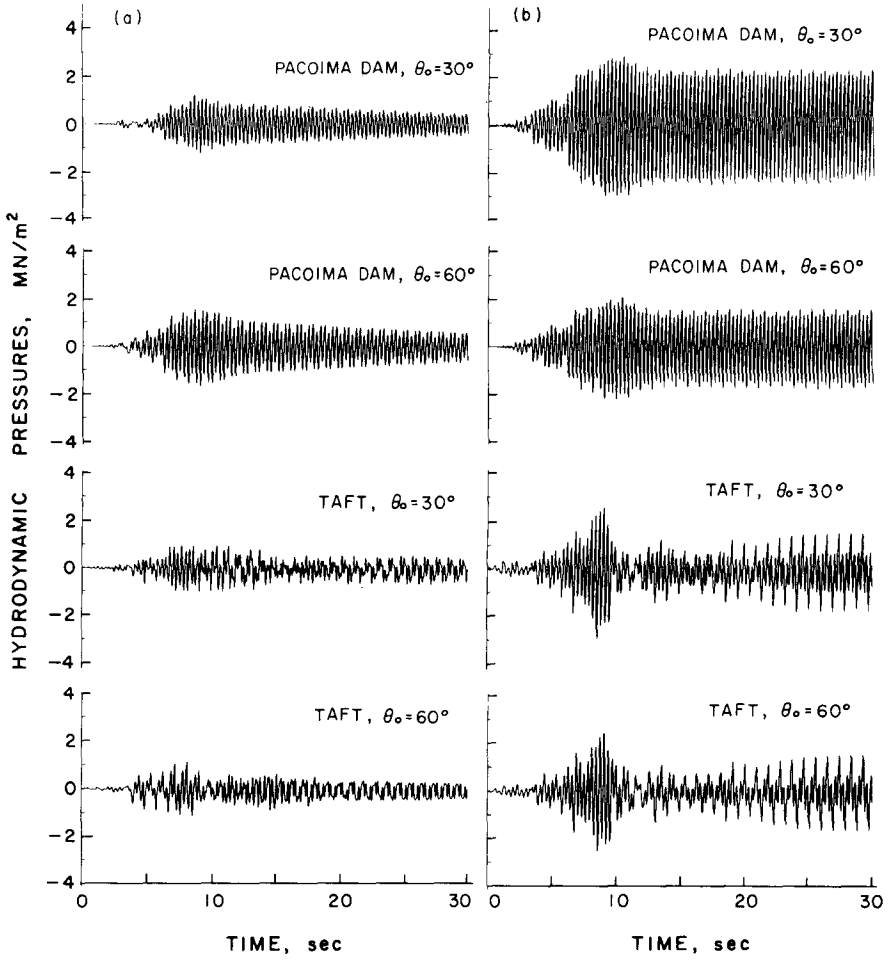

Figure 6. Hydrodynamic pressures at the downstream gate generated by: (a) the horizontal motion of the dam; (b) the vertical motion of the reservoir floor

This is not surprising, because the complex frequency response function [Figure 3(b)] has the broadest peak at this frequency. The pressures obtained from the accelerograms with shifted phase, not shown here, are smaller than for the in-phase motion, shown in Figure 6(a). The highest amplitudes, about 1·8 MN/m^2, are obtained for the 'Pacoima Dam' excitation at incident angle $\theta_0 = 60°$.

Substantially larger pressure amplitudes [shown in Figure 6(b)] result from the vertical motion of the reservoir floor. This is expected if one notices that the complex frequency response function, Figure 3(c), has several broad peaks located at each of the reservoir characteristic frequencies. For the 'Pacoima Dam' accelerograms the pressures oscillate with the second characteristic frequency, while for the 'Taft' accelerogram both first and second modes of vibration are present. The highest amplitudes, reaching 3 MN/m^2 (three times the hydrostatic pressure) are computed for the case of the 'Pacoima Dam' accelerogram with incident angle of $\theta_0 = 30°$. The differences between the pressures computed for in-phase and with phase shifted accelerograms (not shown) are smaller than in the above case.

Total hydrodynamic pressures, shown in Figure 7, are computed by summing up the pressure time histories obtained due to the gate motion, the dam motion and the reservoir floor motion. It is seen that in some cases the amplitudes are larger for the phase shifted than for the in-phase motion at points O and I. For earthquake waves arriving with $\theta_0 = 60°$, the presence of the fundamental frequency of the bottom outlet is noticeable. The

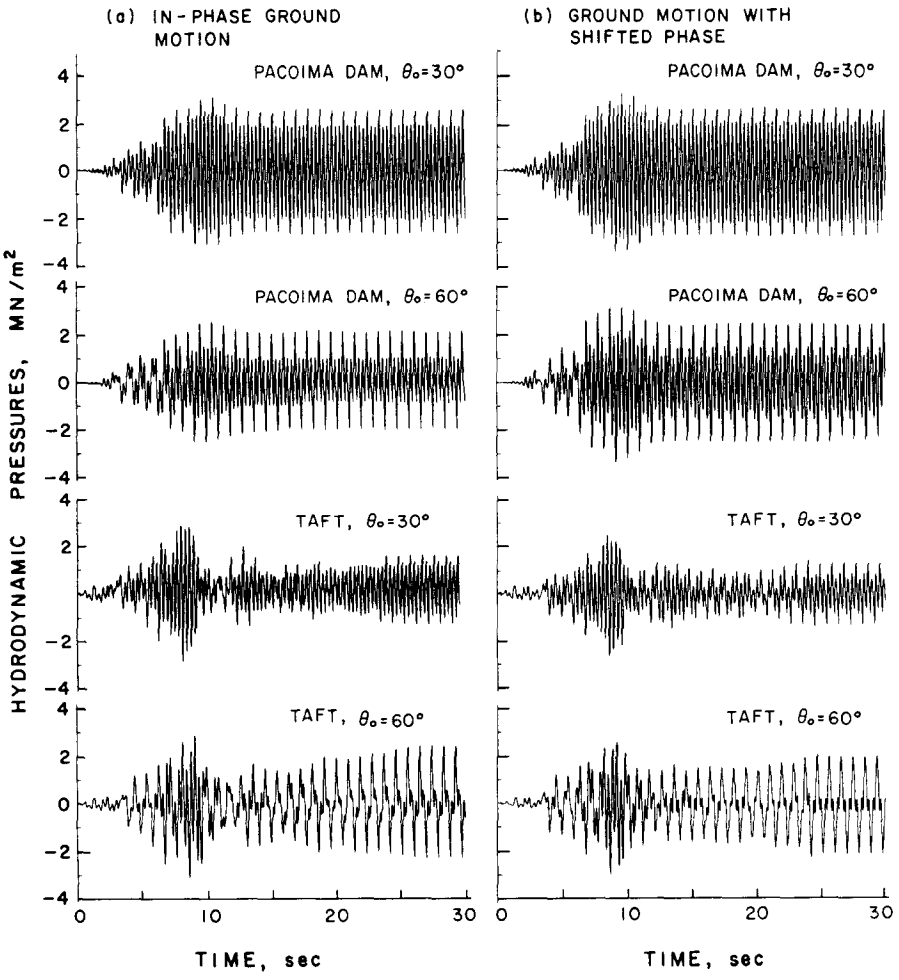

Figure 7. Total hydrodynamic pressures at the downstream gate due to the gate, dam and reservoir floor motions

highest amplitudes, about 3·3 MN/m^2, are obtained for the 'Pacoima Dam' ($\theta_0 = 30°$) accelerogram. All pressure histories have shown no significant amplitudes decaying with time, even after the earthquake motions completely stop. This is because of the small energy dissipation of the pressure waves in the bottom outlet.

Envelopes of the absolute maximum pressures computed from the pressure time histories, at five sections along the bottom outlet, are shown in Figures 8(a) to (e) for the gate, dam and reservoir floor motions, and due to four earthquake excitation cases, discussed above (two with and two without the phase shift). It is noted that the dam motion and the reservoir floor motion increase the hydrodynamic pressures substantially. The phase shift of the accelerograms, caused by the propagation effects from O to I, in some cases decreases the pressures by about 25 per cent [Figures 8(b) and (c)], and in other cases increases the pressures by ~ 10 per cent [Figures 8(d) and (e)]. At the section located at $\frac{1}{4}L$ from the downstream gate, the pressure amplitudes are decreased due to a wave node located near this section.

Envelopes of the total, absolute maximum pressures are shown in Figure 9(a) for in-phase motions and in

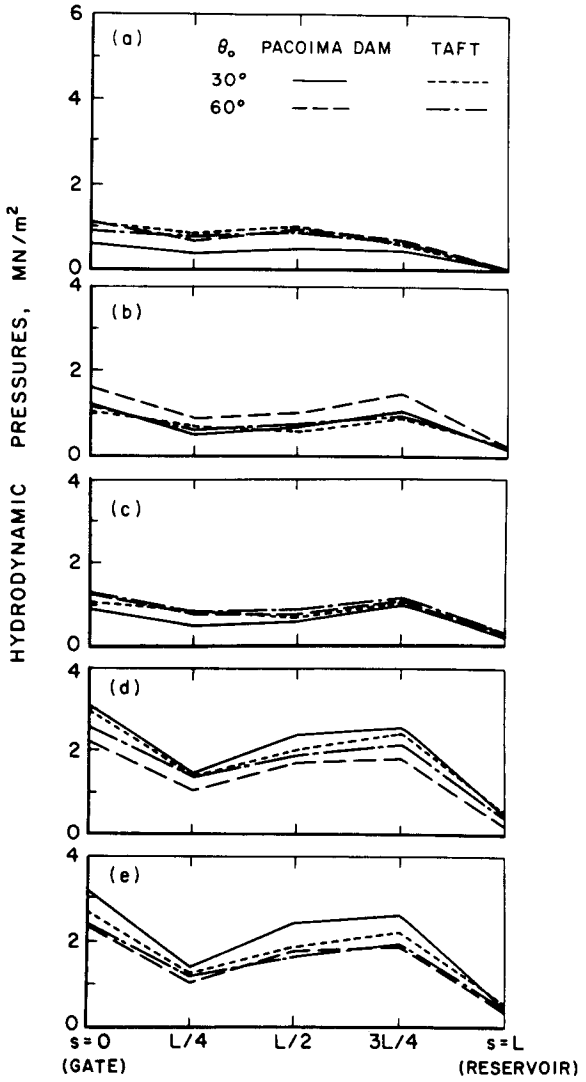

Figure 8. Envelopes of the absolute maximum hydrodynamic pressures along the bottom outlet: (a) horizontal motion of the downstream gate; (b) horizontal in-phase motion of the dam; (c) horizontal motion of the dam with shifted phase; (d) vertical in-phase motion of the reservoir floor; (e) vertical motion of the reservoir floor with shifted phase

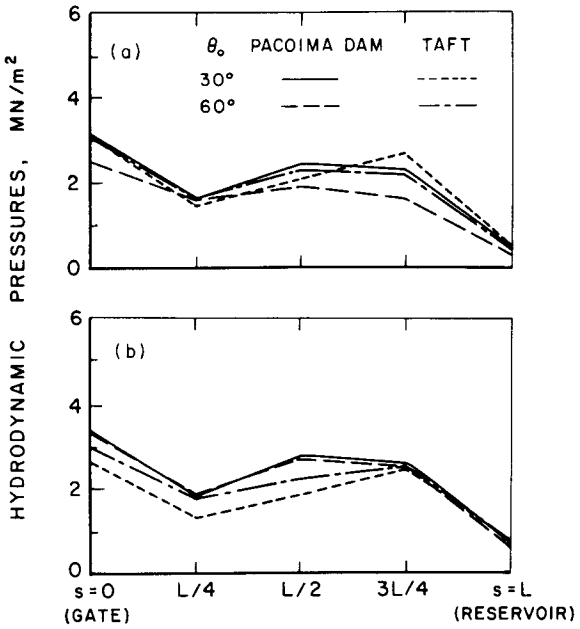

Figure 9. Envelopes of the total, absolute maximum hydrodynamic pressures along the bottom outlet: (a) in-phase motion of the gate, dam and reservoir floor; (b) phase shifted motion of the gate, dam and reservoir floor

Figure 9(b) for the phase shifted excitations. The simulated 'Pacoima Dam' accelerogram ($\theta_0 = 30°$) governs at all sections. In this example for all earthquakes considered and at all sections, except at the bottom outlet entrance, the hydrodynamic pressures range from 1·5 to 3·3 times the hydrostatic pressure of 0·98 MN/m^2. This indicates that, for even moderate earthquakes with peak acceleration $\sim 0{\cdot}2\,g$, large hydrodynamic pressures will be developed within the first several seconds of excitation. This may cause non-linear response of the water (not considered in this analysis) and consequently the walls of the bottom outlet may be exposed to cavitation effects.

CONCLUSIONS

This study examined the phenomenon of the transient pressures in hydrotechnical tunnels generated by earthquakes. The method of the discrete Fourier transform has been applied and is shown to be useful in solving hydraulic transient problems of this type.

An example of the bottom outlet has been investigated. To illustrate the phase delay of the earthquake ground motions between the entrance and the end of the bottom outlet, the recorded accelerograms have been reconstructed through wave propagation effects of P, SV and SH waves in the half space. From the examples analysed, the differences in the hydrodynamic pressures, due to the phase delay of the excitation functions, are 10 to 25 per cent relative to the results computed for the in-phase motions. However, the site specific effects of the wave passage along the long bottom outlet will depend on the details of the local site geology, the ratio of the outlet length L and the wave length of incident waves, and thus may be quite different in each particular case (see for example Moeen-Vaziri and Trifunac[14,15]).

The horizontal motion of the dam and the vertical motion of the reservoir floor have generated the hydrodynamic pressure along the bottom outlet with substantially higher amplitudes than the motion of the downstream gate itself. This is observed especially for the case of the vertical motion of the reservoir floor. In other words, the hydrotechnical tunnel with closed downstream gate and under the reservoir hydrostatic pressure represents an amplifier of the reservoir hydrodynamic pressures caused by earthquakes. Therefore, the upstream boundary conditions cannot be omitted from the analysis of these structures.

Along the length of the bottom outlet, hydrodynamic pressures exceeded the hydrostatic pressure several times. This indicates that, even for moderate earthquakes, cavitation may occur. In this case the bottom outlet lining should be designed to withstand larger positive pressures than those obtained in the linear response analysis, because of the dynamic closure of cavitated regions,[16] and should be adequately stiffened to prevent its buckling under the negative pressure.

The simple mathematical model presented in this paper can be further improved and extended by introducing other boundary conditions, like the surge tank located along the bottom outlet. This may decrease the transient pressures and help decay the pressure oscillations after an earthquake.

ACKNOWLEDGEMENTS

S. B. Kojić is grateful to the University of Southern California, Los Angeles, U.S.A. and Energoproject Co., Hidroingineering Division, Belgrade, Yugoslavia, for their continuous support during this work.

APPENDIX

In Figure 10 the coordinate system at point O (from Figure 1) is repeated with additional designations for the wave amplitudes and angles of incident and reflected waves.

Accelerations due to plane P, SV and SH waves in the elastic half space can be computed from the expressions given for their displacement amplitudes.[11,12] For point I ($DX1, DX2 = 0, DX3$), located at the free surface, the expressions for accelerations $\ddot{U}_i^{P,SV,SH}$ in the $i = 1, 2$ and 3 directions are given in the following. In all subsequent quantities representing the second derivative with respect to time, and designated by $\ddot{U}$ in this Appendix, ω^2 has been set to one and omitted. A_0 was also set equal to one in all calculations, which here address only the relative amplitudes at a given frequency, but at different locations.

Accelerations due to P waves

For $0 \leqslant \theta_0 \leqslant 90°$ accelerations in the $X1$ and $X2$ directions are

$$\ddot{U}_1^P = \{(A_0 \sin\theta_0 + A_1 \sin\theta_1 + A_2 \cos\theta_2) \exp(-\mathrm{i}DX1K_0 \sin\theta_0)\} \exp(\mathrm{i}\omega t) \tag{A1}$$

$$\ddot{U}_2^P = \{(A_0 \cos\theta_0 - A_1 \cos\theta_1 + A_2 \sin\theta_2) \exp(-\mathrm{i}DX1K_0 \sin\theta_0)\} \exp(\mathrm{i}\omega t) \tag{A2}$$

where $\theta_1 = \theta_0$, $\sin\theta_2 = \kappa^{-1} \sin\theta_0$, $\kappa = K_2/K_0$, $K_0 = \omega/c_L$ and $K_2 = \omega/c_T$. ω is the frequency of harmonic waves while c_L and c_T are the velocities of longitudinal and transversal waves, respectively. The amplitude

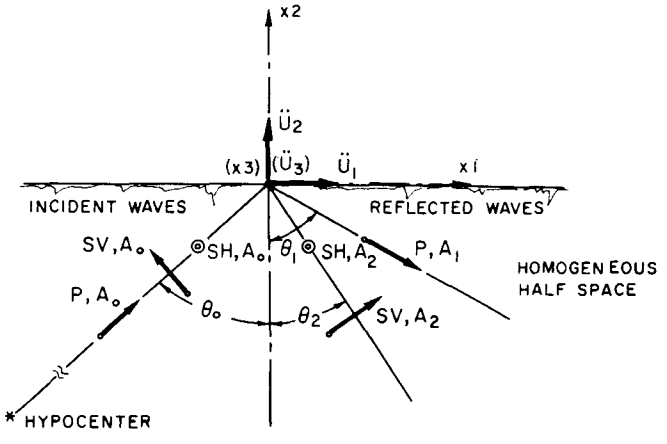

Figure 10. Coordinate system with incident and reflected plane P, SV and SH waves

ratios of the reflected waves and the incident wave are

$$\frac{A_1}{A_0} = \frac{\sin 2\theta_0 \sin 2\theta_2 - \kappa^2 \cos^2 2\theta_2}{\sin 2\theta_0 \sin 2\theta_2 + \kappa^2 \cos^2 2\theta_2} \tag{A3}$$

and

$$\frac{A_2}{A_0} = \frac{2\kappa \sin 2\theta_0 \cos 2\theta_2}{\sin 2\theta_0 \sin 2\theta_2 + \kappa^2 \cos^2 2\theta_2} \tag{A4}$$

Accelerations due to SV waves

When $\theta_0 < \theta_{cr}$ [where $\theta_{cr} = \sin^{-1}(1/\kappa)$], the accelerations are

$$\ddot{U}_1^{SV} = \{(-A_0 \cos\theta_0 + A_1 \sin\theta_1 + A_2 \cos\theta_2) \exp(-iDX1K_0 \sin\theta_0)\} \exp(i\omega t) \tag{A5}$$

and

$$\ddot{U}_2^{SV} = \{(A_0 \sin\theta_0 - A_1 \cos\theta_1 + A_2 \sin\theta_2) \exp(-iDX1K_2 \sin\theta_0)\} \exp(i\omega t) \tag{A6}$$

where $\theta_2 = \theta_0$, $\sin\theta_1 = \kappa \sin\theta_0$, $\kappa = c_L/c_T$, $K_0 = K_2$, and ω, c_L and c_T are as previously defined. The amplitude ratios of the reflected and incident waves are

$$\frac{A_1}{A_0} = \frac{-\kappa \sin 4\theta_0}{\sin 2\theta_0 \sin 2\theta_1 + \kappa^2 \cos^2 2\theta_0} \tag{A7}$$

$$\frac{A_2}{A_0} = \frac{\sin 2\theta_0 \sin 2\theta_1 - \kappa^2 \cos^2 2\theta_0}{\sin 2\theta_0 \sin 2\theta_1 + \kappa^2 \cos^2 2\theta_0} \tag{A8}$$

For $\theta_0 = \theta_{cr}$, $\theta_1 = \pi/2$, and the amplitude ratios become

$$\frac{A_1}{A_0} = \frac{4(\kappa^2 - 1)^{1/2}}{\kappa(2 - \kappa^2)} \tag{A9}$$

$$\frac{A_2}{A_0} = -1 \tag{A10}$$

For the case $\theta_0 > \theta_{cr}$ accelerations are

$$\begin{aligned}\ddot{U}_1^{SV} = \{&-A_0 \cos\theta_0 \exp(-iDX1K_0 \sin\theta_0) + S \sin\theta_1 \exp[-i(DX1K_0 \sin\theta_0 + \alpha)] \\ &- A_0 \cos\theta_2 \exp[-i(DX1K_0 \sin\theta_0 + 2\alpha)]\} \exp(i\omega t)\end{aligned} \tag{A11}$$

and

$$\begin{aligned}\ddot{U}_2^{SV} = \{&A_0 \sin\theta_0 \exp(-iDX1K_0 \sin\theta_0) - S \cos\theta_1 \exp[-i(DX1K_0 \sin\theta_0 + \alpha)] \\ &- A_0 \sin\theta_2 \exp[-i(DX1K_0 \sin\theta_0 + 2\alpha)]\} \exp(i\omega t)\end{aligned} \tag{A12}$$

where $\cos\theta_1 = i(\kappa^2 \sin\theta_0 - 1)^{1/2}$, $\sin\theta_1 = \kappa \sin\theta_0$,

$$S = \frac{-A_0 \sin 4\theta_0}{[\kappa^2 \cos^4 2\theta_0 + 4(\kappa^2 \sin\theta_0 - 1)\sin^2 2\theta_0 \sin^2\theta_0]^{1/2}} \tag{A13}$$

$$\alpha = \tan^{-1} \frac{2(\kappa^2 \sin^2\theta_0 - 1)^{1/2} \sin 2\theta_0 \sin\theta_0}{\kappa \cos^2 2\theta_0} \tag{A14}$$

and

$$\left|\frac{A_2}{A_0}\right| = 1 \tag{A15}$$

Accelerations due to SH waves

This wave causes motion in the $X3$ direction only, so that

$$\ddot{U}_3^{SH} = \{2A_0 \exp[-i(DX1K_0 \sin\theta_0)]\} \exp(i\omega t) \tag{A16}$$

In this case $\theta_2 = \theta_0$, $A_2 = A_0$, $A_1 = 0$ and $K_0 = \omega/c_T$.

Equations (A1), (A2), (A5), (A6), (A11), (A12) and (A16) without $\exp(i\omega t)$ represent the transfer functions, $\ddot{U}_1^{P,SV\text{ or }SH}$ for the harmonic, plane waves in the $i = 1, 2$ and 3 directions at the free surface. These have been used for the modification of the 'Pacoima Dam' and 'Taft' recorded accelerograms. This has been performed by multiplication of the above transfer functions with the corresponding components of recorded accelerograms transferred in the frequency domain, $\bar{a}_{VER}^{P}$, $\bar{a}_{HOR2}^{SV}$ and $\bar{a}_{HOR1}^{SH}$, in the following way:

$$\ddot{U}_1 = \ddot{U}_1^{P}\bar{a}_{VER}^{P} + \ddot{U}_1^{SV}\bar{a}_{HOR2}^{SV} \tag{A17}$$

$$\ddot{U}_2 = \ddot{U}_2^{P}\bar{a}_{VER}^{P} + \ddot{U}_2^{SV}\bar{a}_{HOR2}^{SV} \tag{A18}$$

and

$$\ddot{U}_3 = \ddot{U}_3^{SH}\bar{a}_{HOR1}^{SH} \tag{A19}$$

By the inverse Fourier transform of $\ddot{U}_1$, $\ddot{U}_2$ and $\ddot{U}_3$ the simulated accelerograms are obtained at the specified point on the free surface in the $X1$, $X2$ and $X3$ directions. Applying this procedure it was possible to simulate the delay of ground motion between the intake and the end of the bottom outlet.

REFERENCES

1. O. C. Zienkiewicz, 'Hydrodynamic pressures due to earthquakes', *Water power constr.*, **15**, Sept. (1963).
2. D. Obradović, 'Analysis of transient phenomenon in the bottom outlet of the Haditha Dam' (in Serbocroatian), Report by Energoproject Co., Belgrade, Yugoslavia, Mar. 1982.
3. M. H. Chaudhry, *Applied Hydraulic Transients*, Van Nostrand Reinhold, New York, 1979.
4. V. L. Streeter and E. B. Wylie, *Fluid Mechanics*, 8th edn, McGraw-Hill, New York, 1985.
5. M. D. Trifunac and A. G. Brady, 'Correlations of peak acceleration, velocity and displacement with earthquake magnitude, distance and site conditions', *Earthquake eng. struct. dyn.* **4**, 455–471 (1976).
6. S. H. Crandall and W. D. Mark, *Random Vibration in Mechanical Systems*, Academic Press, New York, 1973.
7. J. F. Hall, 'An FFT algorithm for structural analysis', *Earthquake eng. struct. dyn.* **10**, 797–811 (1982).
8. A. K. Chopra, 'Hydrodynamic pressures on dams during earthquakes', *J. eng. mech. div. ASCE*, **93**, No. EM6, 205–223 (1967).
9. G. Fenves and A. K. Chopra, 'Effects of reservoir bottom absorption and dam–water–foundation rock interaction on frequency response functions for concrete gravity dams', *Earthquake eng. struct. dyn.* **13**, 13–31 (1985).
10. E. Rosenblueth, 'Presión hydrodinámica en presas debida a la aceleración vertical con refracción en al fondó', *2nd natl. cong. sers. eng.* Veracruz, Mexico (1968).
11. J. D. Achenbach, *Wave Propagation in Elastic Solids*, North-Holland, Amsterdam, 1980.
12. M. D. Trifunac, 'A note on rotational components of earthquake motions on ground surface for incident body waves', *Soil dyn. earthquake eng.* **1**, 11–19 (1982).
13. E. O. Brigham, *The Fast Fourier Transform*, Prentice-Hall, Englewood Cliffs, N.J., 1974.
14. N. Moeen-Vaziri and M. D. Trifunac, 'Scattering and diffraction of plane SH waves by two-dimensional inhomogeneities', *Soil dyn. earthquake eng.* (in press).
15. N. Moeen-Vaziri and M. D. Trifunac, 'Scattering and diffraction of plane P and SV waves by two-dimensional inhomogeneities', *Soil dyn. earthquake eng.* (in press).
16. O. C. Zienkiewicz, D. K. Paul and E. Hinton, 'Cavitation in fluid–structure response (with particular reference to dams under earthquake loading)', *Earthquake eng. struct. dyn.* **11**, 463–481 (1983).